

Assessing Whole-Body Absorption Cross Section For Diffuse Exposure From Reverberation Chamber Measurements

Aliou Bamba^{*1}, Davy Gaillot², Emmeric Tanghe¹, Günter Vermeeren¹, Wout Joseph¹ *senior member IEEE*,
Martine Lienard² and Luc Martens¹ *member IEEE*

¹Ghent University / iMinds - Department of Information Technology
Gaston Crommenlaan 8 box 201, B-9050 Ghent-Belgium

Fax: +32 9 33 14 899, Tel: +32 9 33 14 908

*Email: aliou.bamba@intec.ugent.be

²TELICE Group, IEMN, University of Lille
Bât. P3, 59655 Villeneuve d'Ascq, France

Abstract—An original experimental protocol is developed to assess the whole-body absorption cross section of objects with arbitrary shapes and materials in diffuse fields at any operating frequency. This approach is important for dosimetry specifically in realistic environments wherein diffuse fields can be prominent. For this application, the knowledge of the whole-body specific absorption rate is critical and can be determined from the human whole-body absorption cross section. The whole-body absorption cross section is obtained from measurements performed in a stirred-mode reverberating chamber processed with the high-resolution parameter estimator RiMAX. To validate the proposed approach and highlight its robustness, the whole-body absorption cross section of a cylindrical phantom is experimentally and numerically determined at 1800 MHz. For both methods, the whole-body absorption cross section is shown to be independent on the orientation of the transceivers, indicating that it is indeed caused by diffuse fields. A good agreement is obtained between experimental and numerical Finite-Difference Time-Domain (FDTD) results with a relative deviation of about 17 %. From the validation of this approach, the measurement protocol is applied to a real human at 1800 MHz resulting in a whole-body absorption cross section of 0.95 m², 1.01 m² and 1.11 m² for a sitting, standing, and standing with stretched arms posture, respectively.

Keywords: Reverberation chamber, reverberation time, diffuse multipath components, maximum-likelihood high-resolution channel parameter estimator, whole-body absorption cross section, mean absorption cross section, whole-body specific absorption rate, (un)stirred components.

I. INTRODUCTION

REVERBERATION chambers [1]–[6] have been used for the electromagnetic compatibility (EMC) measurements and for the wireless channels characterization. The different sources of losses inside a reverberation chamber are well described in [2]. The plane wave integral representation and properties in a reverberation chamber are addressed in [3]. [4] presented a statistical electromagnetic theory when unstirred components of the electromagnetic field (EMF) are presented in the chamber. [5] described how to tune a reverberation chamber to emulate either a Rayleigh or a Rician channel, along with the probability density function of the EMF. The authors of [6] have shown that the reverberation chamber emulates a rich isotropic multipath environment, which can be considered as an extreme reference for the realistic indoor environments where the scattered waves are prominent. The multiple paths are generated by the reflections of electromagnetic waves (EMW) on the walls and on a mechanical

paddle rotating in the chamber. The multiple paths characteristics enhance the performance of the multiple-input multiple-output (MIMO) channels. Therefore, the reverberation chambers (RCs) are more and more used for the characterization of wireless MIMO channels [7], [8] and for the wireless communication performances evaluation [9], [10]. In addition, RCs are also used to determine the mean absorption cross section (ACS_{mean}) of lossy objects. This information is critical when assessing an antenna radiation efficiency located close to lossy object such as a head phantom [11].

The ACS_{mean} of a lossy object is also used to estimate the loading effects in terms of the average gain in some radio frequency (RF) reverberating environments such as an aircraft passenger cabin [12]. Its determination procedure can be found in [11]–[14]. The notion of the ACS_{mean} is clearly related to the performance of the reverberating environment in terms of averaged gain and is different from the whole-body absorption cross section (ACS_{wb}). Both can be measured in RCs but the ACS_{mean} is obtained from the averaged or mean power whereas the ACS_{wb} is obtained from the summed or integrated power. Recent literature reviews show that the diffuse multipath components (DMC) may contribute significantly (up to 95%) to the total power density involved in some realistic environments [15], [16]. Therefore, the knowledge of the whole-body ACS_{wb} induced by diffuse fields is critical with respect to the experimental investigation of human's specific absorption rate (SAR) in realistic environments [17]. There is a lack of information in the literature regarding the human's ACS_{wb} . [18] developed a method to determine the ACS_{wb} of humans in an office environment. The method presented therein *i)* assumed all the humans under test to have the same ACS_{wb} , and *ii)* did not separate the diffuse fields (stirred energy) from the possible specular components (unstirred energy). It is noteworthy to mention that the terms diffuse and specular are related to the realistic environments whereas the terms stirred and unstirred pertain to the RCs. Removing the unstirred energy from the measurements improves the ACS determination in terms of statistical error [14]. The use of a numerical algorithm such as the maximum-likelihood high-resolution channel parameter estimation RiMAX [19] is expected to provide additional robustness and possibilities since it *i)* removes the unstirred energy from the measurements and *ii)* allows the determination of the ACS_{wb} of a single person,

allowing thereby the investigation of different postures of the human under test.

The novelty of this paper is as follows. Firstly, the whole-body ACS_{wb} is defined and the differences with the mean ACS are outlined. Then, the whole-body ACS_{wb} of a canonical phantom is determined - through measurements in a RC - by using RiMAX. Secondly, the obtained values are compared with the numerical results as a validation. The numerical solution is based on more than 840 FDTD simulations. Thirdly, the method is applied to a real human to determine its ACS_{wb} section at 1800 MHz. The ACS of a lossy object is independent on the reverberating environment [12]. Therefore, the human whole-body ACS_{wb} values obtained experimentally from the RC measurements are used to determine the whole-body specific absorption rate due to the diffuse fields, which may be prominent in realistic reverberating environments such as aircrafts, offices, etc... To the knowledge of the authors, this is the first time where *i*) the whole-body absorption cross section - induced by diffuse fields - is clearly defined and *ii*) the whole-body specific absorption rate is experimentally determined for different postures. The paper is organized as follows: The materials and the methodology are introduced in Section II. The definition of the mean and whole-body absorption cross section are also addressed. Section III presents the measured and simulated results. In Section IV, realistic values of a human whole-body ACS_{wb} are determined from the reverberation chamber measurements and the related whole-body specific absorption rate are also determined. Finally, conclusions are drawn in Section V.

II. MATERIALS AND METHODS

A. Reverberation chamber

A Stirred-Mode Reverberation Chamber (SM-RC) is a fully-closed metallic cavity which is oversized with respect to the investigated wavelength. It operates over a large frequency bandwidth (e.g: 1 - 18 GHz) depending upon its dimensions and volume. Due to the cavity effect, there exists a working volume sufficiently separated from the walls wherein the electromagnetic fields are statistically uniform for all measurement points, directions, and electromagnetic emitting source positions. A rotating twisted metallic sheet inside the chamber provides the stirring of the electromagnetic modes.

The RC dimensions are 2.8 m \times 5.7 m \times 4.1 m (Height \times Length \times Width) and 65 m³ volume. A metallic sheet is mounted onto a vertical pole going from the ceiling to the floor and consists of 4 vertical elements [8]. Figure 1 shows the reverberation chamber.

B. Materials and measurement setup

The study has been carried out at the 1800 MHz (telecommunication frequency and future Long-Term Evolution frequency in Belgium, Italy, Germany, United Kingdom, etc...) within a bandwidth of 100 MHz divided into 101 frequency points. As transceivers, two Double Ridge Guide Horn Antennas of type SAS-571 were placed in the RC in order to achieve a Rayleigh channel. Three orientations of the transceivers are considered. For the vertical orientation, the Tx and the Rx feeder are both oriented along the z-axis direction (referring to the coordinates system in Fig. 1); for the horizontal polarization, the Tx and the Rx feeder are both oriented along the y-axis direction; and finally for the cross orientation, the Tx feeder (resp. the Rx

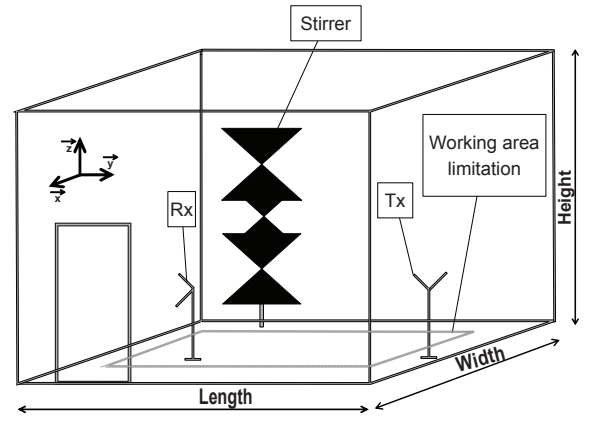


Fig. 1. Illustration of the reverberation chamber

feeder) is oriented along the y (resp. z) axis direction. The stirrer rotates 180 times during one measurement with a step of 2°. For each of its positions, the impulse transfer function of the propagation channel is measured; the power delay profile (PDP) being calculated from it.

The experiments have been performed with four identical polyvinyl chloride (PVC) cylindrical phantoms positioned arbitrarily in the working area of the RC. The phantom has an inner radius of 119.5 mm, an outer radius of 124.5 mm (thickness = 5 mm) and a height of 1500 mm. Dosimetric measurements are usually performed with liquids having dielectric properties similar to those of biological tissues. Hence, a tissue simulating liquid that has the similar dielectric properties as the body tissue parameters specified in [20] is used. The liquid has a relative complex permittivity $\epsilon_r = 57.74 + j*13.55$, conductivity $\sigma = 1.47$ S/m, and mass density of $\rho = 1000$ kg/m³. The liquid is used in the experiments and its properties included into all the simulations as well. The dielectric properties of the liquid were measured using a Hewlett Packard HP85070A dielectric probe kit connected to a Hewlett Packard HP8753D network analyzer [21]. All the measurements in the RC were carried out the same day in order to avoid excessive evaporation of the liquid. In addition, we ensured that the dielectric properties variations were within ± 5 %, as recommended in [22].

C. Experimental Whole-body absorption cross section determination

Channel parameters estimation algorithm: Recent studies have shown that the wireless narrow band radio channel h can be considered as a superposition of deterministic specular components $s(\Theta_{sc})$ and stochastic dense multipath components $d(\Theta_{dmc})$, which include diffuse components [19], [23], [24]. Here, Θ_{sc} and Θ_{dmc} are the set of parameters that fully describe the propagation mechanisms:

$$h = s(\Theta_{sc}) + d(\Theta_{dmc}) \quad (1)$$

The sampled response vector $h \in \mathbb{C}^{M_f \times 1}$ (where M_f corresponds to the number of frequency points) is assumed to follow a multivariate circular symmetric complex Gaussian process with mean $s(\Theta_{sc})$ and covariance $R(\Theta_{dmc})$:

$$h \approx N_c(s(\Theta_{sc}), R(\Theta_{dmc})) \quad (2)$$

As illustrated in Fig. 2-4 of [19] and in Fig. 2 of [25], the DMC power $\psi(\tau)$ as function of time delay τ is described by an exponential decay:

$$\psi(\tau) = \alpha_1 e^{-\frac{(\tau-\tau_d)}{\tau_i}} + \alpha_0, \quad (3)$$

where α_0 is the noise floor in the measured Power Delay Profile (PDP), τ_d is the arrival time of the first DMC, α_1 is the power of the DMC at $\tau=\tau_d$ (typically the highest value of the DMC in the PDP), and τ_i is the reverberation time of the room. α_1 , τ_i , τ_d , and α_0 are the four parameters that fully describe the DMC (see Fig. 2-4 of [19]) and are gathered into the DMC parameter vector. Hence, the covariance matrix of the sampled channel can also be seen as corrupting colored noise and is solely dependent on the diffuse multipath components and additive white noise. This parametric description of the channel enables the use of maximum-likelihood high-resolution channel parameters estimation algorithm. For instance, the estimation of the weak specular and diffuse multipath component parameters was performed in this study with the recently developed RiMAX estimator [23], [24].

The first step towards the experimental assessment of the whole-body ACS_{wb} is to determine the reverberation time τ_i , which is actually the decay rate of the DMC and is proportional to the slope of the decaying tail of the PDP [18]. The total absorbing area in the chamber and its reverberation time are related via the following equation [17], [18], [25], [26]:

$$A' = \frac{4V}{c_0 \tau_i} \quad (4)$$

where A' , V , and c_0 are the effective absorbing area in the chamber, the chamber volume, and the light velocity in the vacuum ($c_0 = 3 \times 10^8$ m/s), respectively.

Next, by varying the reverberation chamber load, the whole-body ACS_{wb} of the object under test is then determined from the different reverberation times values [17], [18].

In addition, the whole-body ACS_{wb} of the object under test i.e., the cylindrical phantom, is computed through numerical simulation for the sake of comparison.

D. Numerical simulation settings

The Finite-Difference Time-Domain (FDTD) solver SEMCAD-X is used to compute numerically the whole-body ACS_{wb} of the phantom. The whole-body ACS_{wb} is determined from the whole-body specific absorption rate (SAR_{wb}) value obtained when the object under test is illuminated simultaneously by several plane waves incident in all directions. The dielectric properties of the liquid described in Section II-B were used for the simulation settings.

Rectangular plane wave sources based on the Total-Field Scattered-field (TFSF) technique [27] are used to excite the object under test, i.e., the cylindrical phantom. The plane waves superposition principle [3] is applied to simulate in SEMCAD-X the multiple paths encountered in a reverberation chamber as it is done in [28], [29]. The multiple waves resulting from a movement of the stirrer is called here a set of waves. M sets are used to excite the cylinder since the stirrer occupied several positions during the measurement. The M sets allow us to derive statistical properties of the whole-body ACS_{wb} because one whole-body ACS_{wb} value is obtained per set. Let us now define the properties of the plane waves within

a set. A set is comprised of N plane waves, i.e., N_a plane waves in the azimuthal domain and N_e elevation angles is considered per azimuth ($N=N_a \times N_e$). The plane waves are uniformly distributed in both azimuthal and elevation domain. The uniform distribution of the EMFs in the azimuthal plane in indoor environments is generally accepted [30]. The total power density is divided by the number of plane waves in a set such that each plane wave has the same amplitude. We expect the polarization to have no preference in diffuse fields. Therefore, the polarization of each plane wave is randomly chosen with equal probability in such a way that half of the total received power would be received by a vertically-polarized antenna and the other half by a horizontally-polarized antenna. Regarding the plane waves phase, the notion of *start point* is rather used [29]. Anyway, the starting point is related to the phase. It is important to mention that when the phase is randomly drawn with equal probability in the range $[0, 2\pi]$, the numerical results do not match the experimental ones when it comes to emulate the electromagnetic waves propagation in reverberation chambers [29]. Here, the starting point of each plane wave is randomly chosen with equal probability in the range $[0, \lambda/2]$; this is the correlation interval [31] ensuring that the E-field values of a plane wave traveling from the start point to the simulation domain will be correlated. Simulation of the

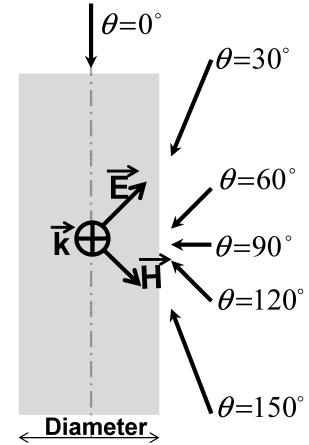


Fig. 2. Cylinder and the diffuse fields illustration (for a given azimuth). 6 elevation angles are considered per azimuth and 72 azimuthal angle are considered. \vec{E} , \vec{H} , and \vec{K} are the electric field vector, magnetic field vector, and wave vector, respectively.

reverberation chamber in SEMCAD-X would have required excessive memory resources and time because the FDTD method would have spatially discretized the entire chamber. Therefore, the object under test is located inside a simulation domain, which has comparable sizes with the object under test. To avoid the reflections of the waves impinging on the simulation domain boundaries, uniaxial perfectly match layer (UPML) is used as absorbing boundaries conditions in such a way that more than 95% of the incident wave power is absorbed by the boundary layers.

The whole-body ACS_{wb} of the object under test is derived from the simulated whole-body SAR_{wb} as follows:

$$ACS_{wb} = \frac{SAR_{wb} \times W}{I} \quad (5)$$

where SAR_{wb} , W , and I are the whole-body specific absorption rate of the object under test in diffuse fields, the object weight,

and the total power density, respectively. It is important to mention once more that the term whole-body refers to the direction of the incoming waves, i.e., the diffuse fields coming simultaneously from all directions.

Because of the randomness introduced by the arbitrary choice of the waves phases and polarizations, the whole-body ACS_{wb} is addressed with a stochastic approach. The statistical multipath tool of Vermeeren et al. [32] - which is based on FDTD simulations - is used to determine the numerical averaged whole-body ACS_{wb} . Regarding the numerical simulation of the cylinder in SEMCAD-X, we set the parameters N_a and N_e defined in Section II-D as follows: $N_a=72$ and $N_e=6$. Each polarization angle in the tool is decomposed into two orthogonal polarizations, leading to a total SEMCAD-X simulations of 842 ($72 \times 6 \times 2$). For the exposure samples, 1000 sets were used to obtain statistical relevant values where each set contains 432 plane waves ($N_a \times N_e$). The statistical multipath tool [32] has the advantage to *i*) reduce considerably the simulations time, and *ii*) facilitate the management of the simulation outcome. The outcome of the tool is the cumulative distribution function (cdf) of the whole-body SAR_{wb} from which it is straightforward to derive the whole-body ACS_{wb} , see (5).

E. Mean (or averaged) absorption cross section and whole-body absorption cross section

Basically, the ACS of a lossy object is defined as the ratio of the power absorbed by the object to the incident power density. However, it is important to make the distinction between the whole-body ACS_{wb} and the mean or averaged ACS_{mean} .

On the one hand, the *mean or averaged absorption cross section* is found by averaging the ACS obtained from a *single* incident plane wave drawn from a uniform distribution in space [11], [33]. An averaging over all the polarizations is also necessary to discard the polarization imbalance [34] of the ACS. The experimental methodology consists in measuring the averaged power levels in steady state - through Hill's formula [2] - of the chamber when it is unloaded and loaded.

The ACS_{mean} of a human (weight ≈ 75 kg and height ≈ 181 cm) determined in a RC from 1 GHz to 8 GHz in a sitting posture was reported in [14].

On the other hand, the *whole-body absorption cross section* is found by calculating the ACS for several plane waves incident *simultaneously* to the object under test. The polarization and the phase of the EMF are both assumed to be random.

To show a clear difference between the two quantities, let us consider an uniform sphere. We will determine in the following section the ACS_{mean} and the ACS_{wb} of an uniform sphere.

1) *Mean absorption cross section of a sphere*: Figure 3(a) shows the configuration of the sphere and an incident plane wave to determine the ACS_{mean} . The radius of the sphere is set to 19.25 cm as in [14] for comparison purpose. The same dielectric properties defined in Section II-B are used at the frequency of 1800 MHz. The ACS_{mean} of a sphere is the same as the ACS for any incoming plane wave [11]. No averaging over the directions nor the polarizations is needed due to the symmetry of the sphere for all directions [33]. The ACS_{mean} of a sphere is analytically determined from the coefficients of the Mie theory [35] and is given by [35, page 103]:

$$ACS_{mean} = ACS_{ext} - ACS_{sca}, \quad (6)$$

where ACS_{ext} and ACS_{sca} are the extinction and scattering ACS respectively, and defined as follows:

$$ACS_{ext} = \frac{2\pi}{k^2} \sum_{n=1}^{\infty} (2n+1) [Re(a_n + b_n)], \quad (7)$$

$$ACS_{sca} = \frac{2\pi}{k^2} \sum_{n=1}^{\infty} (2n+1) [|a_n|^2 + |b_n|^2], \quad (8)$$

where $k = \frac{2\pi}{\lambda}$ is the wavenumber, $Re(X)$ denotes the real part of the complex number X , and a_n and b_n represent the magnetic and electric multi poles of order n , respectively. Their expressions can be found in [35, page 100].

Applying (6), a ACS_{mean} of 0.0695 m^2 is obtained. Similar value of the ACS_{mean} calculated with the Mie theory equations is found at the same frequency, i.e., 1800 MHz and for the same sphere [14]. Here, the ACS_{mean} value obtained from the Mie theory is a reference value since it is obtained from an analytical solution. However, it is note worthy that we obtained a simulated ACS_{mean} (sphere illuminated with a single plane wave) of 0.0684 m^2 , resulting in a deviation of less than 2 %. This excellent agreement between simulation and analytical result is interpreted as an alternative to determine accurately through simulations the ACS of objects with irregular shapes.

2) *Whole-body absorption cross section of a sphere*: The whole-body ACS_{wb} of the same sphere is numerically determined. Figure 3(b) shows the modeling of the diffuse fields in the simulation tool. Here, 200 sets are used for the simulation of the sphere and a set is comprised of 100 plane waves surrounding the sphere. Applying (5) to the 200 whole-body SAR_{wb} values obtained from the statistical tool (mass of 30 kg of the sphere), an averaged whole-body ACS_{wb} of 0.22 m^2 is obtained. The difference between the ACS_{mean} and the averaged whole-body ACS_{wb} is about 4.87 dB, indicating thereby that the two terms are different.

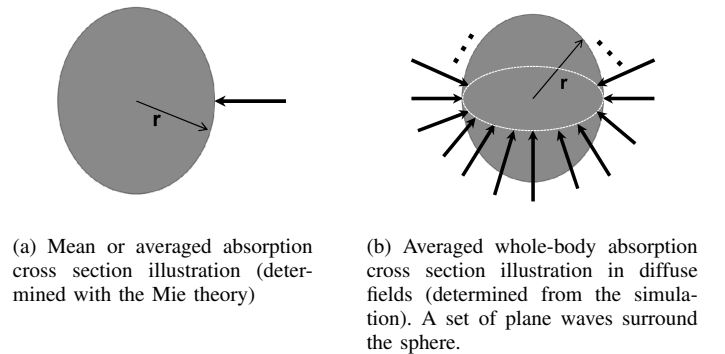


Fig. 3. Difference between the mean and whole-body absorption cross section modeling. The arrows represent the incident plane waves.

III. RESULTS

A. Experimental results

For the experiments, the RC was loaded with 0, 1, 2, 3, or 4 phantom(s) filled with the tissue equivalent liquid, and 180 channel transfer functions were measured for each scenario. The PDPs obtained after taking the squared modulus of the inverse Fourier transformation of the transfer functions were averaged and are shown in Fig. 4. Note from Fig. 4 that the received power does not reach the steady state. This is due to

the small duration of the transmitted pulse. The more phantoms

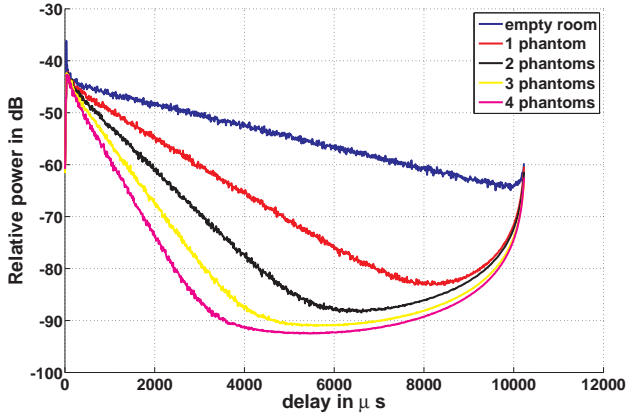


Fig. 4. PDP in the reverberation chamber loaded with a different number of phantom(s) (Vertical-Vertical polarization)

in the RC (i.e. the more loaded), the steeper is the slope of the PDP showing the fast decrease of the DMC power. Physically, the EMF strength decays faster because the area (added cylinders) absorbing the EM radiations is larger. For each PDP, the reverberation time is determined using the RiMAX estimator which removes beforehand any possible unstirred components. The resulting reverberation times are listed in Table I, where τ_i is the reverberation time of the RC loaded with i phantom(s), $i \in \{0, 1, \dots, 4\}$. We observe that the reverberation time depends

Tx-Rx orientation	τ_0 (ns)	τ_1 (ns)	τ_2 (ns)	τ_3 (ns)	τ_4 (ns)	ACS_{wb} (m ²)
vertical (V-V)	2080	823	525	376	296	0.628
cross (V-H)	2125	826	523	376	296	0.628
horizontal (H-H)	2067	823	522	374	295	0.630

TABLE I
REVERBERATION TIMES OF THE CHAMBER AS A FUNCTION OF THE LOAD FOR 3 DIFFERENT POLARIZATIONS ALONG WITH THE CORRESPONDING WHOLE-BODY ABSORPTION CROSS SECTION.

slightly on the transceiver's orientation, but these differences might be due to the measurements uncertainties. From the reverberation time values, the experimental whole-body ACS_{wb} of the cylinder is subsequently obtained - for each orientation of the transceivers - by linear regression of the different absorbing areas [18]. The experimental whole-body ACS_{wb} values are listed in the last column of Table I. The whole-body ACS_{wb} obtained for the different orientations of the transceivers are similar. The maximum difference is lower than 0.4 % and is attributed to the measurements uncertainties. Therefore, the averaged value is retained as the experimental whole-body ACS_{wb} . This result shows that the whole-body ACS_{wb} determined experimentally in the RC is independent on the transceivers orientation, indicating that the whole-body ACS_{wb} is induced by stirred fields and is isotropic.

B. Numerical results

The outcome of the statistical multipath tool is the cdf of the whole-body SAR_{wb} of the cylinder under diffuse exposure, and is shown in Fig. 5. Given its mass of 65 kg - and applying (5) to Fig. 5 - the cdf of the whole-body ACS_{wb} of the cylinder is

obtained and is shown in Fig. 6. From the cdf, an average value of the whole-body ACS_{wb} of 0.52 m² is obtained.

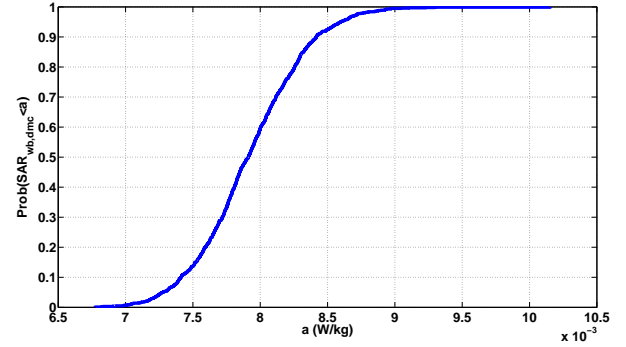


Fig. 5. Cumulative distribution of the whole-body specific absorption rate of the cylinder in diffuse fields.

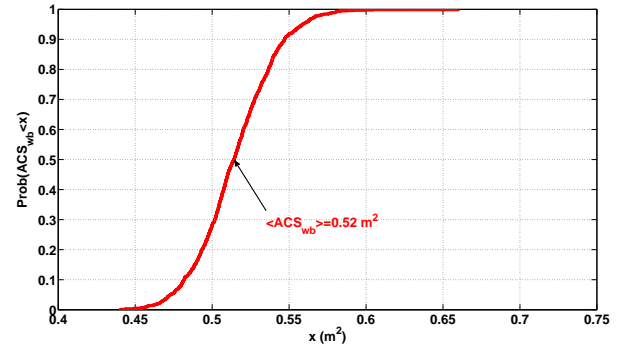


Fig. 6. Cumulative distribution function of the whole-body absorption cross section of the cylinder in diffuse fields.

Table II lists the experimental ACS_{wb} values along with the relative deviations. The relative deviation δ_{ACS} is defined as the difference in percentage between an experimental value and the averaged numerical result in terms of whole-body ACS_{wb} .

Tx-Rx orientation	vertical	cross	horizontal
ACS_{wb}^{exp} (m ²)	0.628	0.628	0.630
δ_{ACS} (%)	17.20	17.20	17.46

TABLE II
CYLINDER EXPERIMENTAL WHOLE-BODY ABSORPTION CROSS SECTION AND THE RELATIVE DEVIATION FROM THE NUMERICAL AVERAGED VALUE

We found numerically (resp. experimentally) an average whole-body absorption cross section of about 0.52 m² (resp. 0.63 m²), leading to a relative deviation of 17 %, indicating a good agreement between the two approaches. The difference between the two approaches is attributed to *i*) the modeling of the incident multiple paths since we only consider few incident angles, *ii*) the statistical properties of the plane waves during the simulations might be slightly different from what actually occurs in the reverberation chamber and *iii*) to other uncertainties during both the measurements and the simulations.

IV. APPLICATION TO A REAL HUMAN

In this Section, the ACS_{wb} of a real human is determined. The person (1.73 m and 63 kg) was located in the RC during the

measurements. Three postures were considered: sitting, standing, and standing with stretched arms.

The whole-body ACS_{wb} is determined for a cross orientation of the transceivers. Two measurements have been carried out: one PDP measurement in the empty RC and a second with the human adopting one of the mentioned postures. The reverberation times are determined with the RiMAX algorithm and are used to assess the human whole-body ACS_{wb} .

As shown in Table III, a human whole-body ACS_{wb} of 0.95 m^2 , 1.01 m^2 , and 1.11 m^2 was obtained for the sitting, standing, and standing with stretched arms postures, respectively. The




Posture			
ACS_{wb}	0.95 m^2	1.01 m^2	1.11 m^2

TABLE III
HUMAN WHOLE-BODY ACS_{wb} FOR DIFFERENT POSTURES

body surface area of a human is only dependent on its weight and height [36]. However, the human whole-body ACS_{wb} for a given configuration of the EMF depends not only on the body surface area but also on the person's posture since the human body surface illuminated by the EMF vary with the posture. The highest ACS_{wb} occurs for the standing with stretched arms posture whilst the lowest occurs for the sitting posture. The obtained values are logically proportional to the effective surface of the human in the three postures. It is noteworthy that these values will change if another frequency is considered.

The ACS is independent on the reverberating environment wherein it is determined [12]. Therefore, the values obtained in a RC can be used to determine the SAR_{wb} due to diffuse fields in realistic reverberating environments. The diffuse power density in an aircraft is addressed in [37] and [18] investigated the diffuse power density in an office environment.

In this work, a diffuse power density of 1 W/m^2 is assumed and the SAR_{wb} of the person under test is determined from (5). Given the experimental ACS_{wb} obtained in the RC, the person's weight (63 kg) and the power density, a SAR_{wb} of about 15.10 mW/kg , 16 mW/kg , and 17.60 mW/kg are obtained for the sitting, standing, and standing with stretched arms postures, respectively. Several studies addressed numerically the SAR in heterogeneous phantoms [38]–[41]. However, it is not fair to compare those results with the SAR_{wb} values determined in diffuse fields since the illuminated surface is different in both cases (see Fig 3). The numerical SAR values in [38]–[41] account for one plane wave, with a vertical or horizontal polarization whilst the SAR_{wb} due to the diffuse fields is determined for several plane waves incident to the person under test, and random polarizations and phases are assumed.

Here, the SAR_{wb} values are provided for realistic environments, i.e., offices, aircrafts, where the diffuse fields are prominent.

V. CONCLUSIONS

The knowledge of the ACS_{wb} is critical for the human SAR assessment in realistic environments. In this work, an original experimental approach is developed to determine the

ACS_{wb} with good accuracy from measured transfer functions at any frequency in a stirred-mode reverberation chamber. To demonstrate the effectiveness and robustness of the proposed method, the ACS_{wb} of a cylindrical phantom was experimentally determined at 1.8 GHz in a reverberation chamber using the high-resolution parameter estimator RiMAX; RiMAX removing the possible unstirred components from the measurements. A good agreement is obtained between experimental measurements and numerical simulations with a 17 % deviation between both methods. Following the validation of the experimental procedure, the ACS_{wb} of a human body was determined for three different postures. Assuming a diffuse power density of 1 W/m^2 , the SAR_{wb} of a human under test was derived for all considered postures. Future research may address the investigation of the human ACS_{wb} as a function of the human body surface area and frequency. The present work clearly demonstrates the potential use of reverberation chambers in the domain of human exposure in real environments where the diffuse fields are prominent.

REFERENCES

- [1] Paolo Corona, Gaetano Latmiral, Enrico Paolini, and Luigi Piccioli. Use of a Reverberating Enclosure for Measurements of Radiated Power in the Microwave Range. *IEEE Transactions on Electromagnetic Compatibility*, 18 (2): pages 54–59, 1976.
- [2] David A. Hill, MArk T. Ma, and Arthur R. Ondrejka. Aperture Excitation of Electrically Large, Lossy Cavities. *IEEE Trans. on Electromagn. Compat.*, 36 (3): pages 169–178, 1994.
- [3] David A. Hill. Plane Wave Integral Representation for Fields in Reverberation Chambers. *IEEE Trans. on Electromagn. Compat.*, 40 (3): pages 209–217, 1998.
- [4] Paolo Corona, Giuseppe Ferrara, and Maurizio Migliaccio. Reverberating Chamber Electromagnetic Field in Presence of an Unstirred Component. *IEEE Trans. on Electromagn. Compat.*, 42 (2): pages 111–115, 2000.
- [5] Christopher L. Holloway, David A. Hill, John M. Ladbury, Perry F. Wilson, Galen Koepke, and Jason Coder. On the Use of Reverberation Chambers to Simulate a Rician Radio Environment for the Testing of Wireless Devices. *IEEE Trans. Antennas Propag.*, 54 (11): pages 3167–3177, 2006.
- [6] Per-Simon Kildal, Charlie Orlenius, and Jan Carlsson. OTA Testing in Multipath of Antennas and Wireless Devices With MIMO and OFDM. *Proceedings of the IEEE*, 100 (7): pages 2145–2157, 2012.
- [7] M. Liénard and P. Degauque. Simulation of dual array multipath channels using mode-stirred reverberation chambers. *Electronics Letters*, 40(10): pages 578–580, 2004.
- [8] O. Delangre. *Caracterisation et Modelisation du Canal Radio en Chambre Reverberante*. PhD thesis, Universite Libre de Bruxelles (Departement OPERA) & Universite Lille 1 (Laboratoire IEMN-TELICE), 2009.
- [9] Per-Simon Kildal. Correlation and Capacity of MIMO systems and Mutual Coupling, Radiation Efficiency, and Diversity Gain of Their Antennas: Simulations and Measurements in a Reverberation chamber. *IEEE Communications Magazine*, 42 (12): pages 104–112, 2004.
- [10] Miguel A. Garca-Fernndez, Juan D. Sanchez-Heredia, Antonio M. Martinez-Gonzlez, David A. Snchez-Hernndez, and Juan F. Valenzuela-Valds. Advances in Mode-Stirred Reverberation Chambers for Wireless Communication Performance Evaluation. *IEEE Communications Magazine*, 49 (7): pages 140–147, 2011.
- [11] U. Carlberg, P. S. Kildal, A. Wolfgang, O. Sotoudeh and C. Orlenius. Calculated and Measured Absorption Cross Sections of Lossy Objects in Reverberation Chamber. *IEEE Transactions on Electromagnetic Compatibility*, 46(2): pages 146–154, 2004.
- [12] Nguyen T. RF Loading Effects of Aircraft Seats in an Electromagnetic Reverberating Environment. In *18th Digital Avionics Systems Conference, Proceedings, vol. 2, pages 10.B.5-1 - 10.B.5-7*, 1999.
- [13] Emmanuel Amador, Mihai Ionut Andries, Christophe Lemoine and Philippe Besnier. Absorbing Material Characterization in a Reverberation Chamber. In *10th International Symposium on Electromagnetic Compatibility (EMC Europe)*, pages 177–122, 2011.
- [14] Gregory C. R Melia, Ian D. Flintoft and Martin P. Robinson. Absorption Cross-Section of the Human Body in a Reverberant Environment. In *International Symposium on Electromagnetic Compatibility (EMC EUROPE)*, 2012.
- [15] N. Czink, A. Richter, E. Bonek, J. P. Nuutinen, J. Ylitalo. "Including Diffuse Multipath Parameters in MIMO Channel Models". In *IEEE 66th Vehicular Technology Conference, VTC-2007 Fall.*, 2007.

- [16] J. Poutanen, J. Salmi, K. Haneda, V. M. Kolmonen, and P. Vainikainen. "Angular and Shadowing Characteristics of Dense Multipath Components in Indoor Radio Channels". *IEEE Transactions on Antennas and Propagation*, 59: pages 245–253, 2011.
- [17] A. Bamba, W. Joseph, G. Vermeeren, E. Tanghe, D. P. Gaillot, J. B. Andersen, J. Ø. Nielsen, M. Lienard and L. Martens. Validation of Experimental whole-body SAR Assessment Method in a Complex Environment. *Bioelectromagnetics*, 34 (2): pages 122–132, 2013.
- [18] A. Bamba, W. Joseph, J. B. Andersen, E. Tanghe, G. Vermeeren, D. Plets, J. O. Nielsen, and L. Martens. Experimental Assessment of Specific Absorption Rate Using Room Electromagnetics. *IEEE Transactions on Electromagnetic Compatibility*, 54 (4): pages 747–757, 2012.
- [19] A. Richter. *Estimation of Radio Channel Parameters: Models and Algorithms*. PhD thesis, Faculty of electrical Engineering and Information Technology at the Technical University. Ilmenau, Germany., 2005.
- [20] D. L. Means and K. W. Chan. Evaluating Compliance with FCC Guidelines for Human Exposure to Radiofrequency Electromagnetic Fields. Technical report, Federal Communications Commission Office of Engineering & Technology, 2001.
- [21] W. Joseph and L. Martens. Comparison of Safety Distances Based on the Electromagnetic Field and Based on the SAR for Occupational Exposure of a 900-MHz Base Station Antenna. *IEEE Transactions on Electromagnetic Compatibility*, 47 (4): pages 977–985, 2005.
- [22] *IEEE Recommended Practice for Determining the Peak Spatial-Average Specific Absorption Rate (SAR) in the Human Head from Wireless Communications Devices: Measurement Techniques*, 2003.
- [23] A. Richter, M. Landmann, R.S. Thoma. Parameter Estimation Results of Specular and Dense Multipath Components in Micro- and Macro-Cell Scenarios. In *Proc. WPMC 2004, Abano Terme, Italy, September 2004.*, 2004.
- [24] Andreas Richter, and Reiner S. Thoma. Joint Maximum Likelihood Estimation of Specular Paths and Distributed Diffuse Scattering. In *61st IEEE Vehicular Technology Conference, VTC 2005-Spring, pages 11-15 vol. 1.*, 2005.
- [25] A. Bamba, W. Joseph, E. Tanghe, G. Vermeeren and L. Martens. Circuit Model for Diffuse Multipath and Electromagnetic Absorption Prediction in Rooms. *IEEE Transactions on Antennas and Propagation*, 61 (6): pages 3292–3301, 2013.
- [26] J. Bach Andersen, J. Ø. Nielsen, G. F. Pedersen, G. Bauch, and M. Herdin. "Room Electromagnetics". *IEEE Antennas Propag. Mag.*, 49, no. 2: pages 27–33, 2007.
- [27] F. W. Smith D. E. Merewether, R. Fisher. On Implementing a Numeric Huygen's Source Scheme in a Finite Difference Program to Illustrate Scattering Bodies. *IEEE Trans. Nucl. Sci.*, 27 (6): pages 1829–1833, 1980.
- [28] Franco Moglie, and Anna Pia Pastore. FDTD Analysis of Plane Wave Superposition to Simulate Susceptibility Tests in Reverberation Chambers. *IEEE Transactions on Electromagnetic Compatibility*, 48 (1): pages 195–202, 2006.
- [29] Valter Mariani Primiani and Franco Moglie. Numerical Simulation of Reverberation Chamber Parameters Affecting the Received Power Statistics. *IEEE Transactions on Electromagnetic Compatibility*, 54 (3): pages 522–532, 2012.
- [30] Kimmo Kalliola, Kati Sulonen, Heikki Laitinen, Outi Kivekas, Joonas Krogerus, and Pertti Vainikainen. Angular Power Distribution and Mean Effective Gain of Mobile Antenna in Different Propagation Environments. *IEEE Trans. Veh. Technol.*, 51 (5): pages 823–838, 2002.
- [31] David A. Hill. Spatial Correlation Function for Field in a Reverberation Chamber. *IEEE Transactions on Electromagnetic Compatibility*, 37: pages 138–145, 1995.
- [32] G. Vermeeren, W. Joseph, C. Olivier, and L. Martens. Statistical multipath exposure of a human in a realistic electromagnetic environment. *Health Physics*, 94, no. 4: pages 345–354, April 2008.
- [33] Christopher L. Holloway, David A. Hill, John M. Ladbury and Galen Koepke. Requirements for an Effective Reverberation Chamber: Unloaded or Load. *IEEE Transactions on Electromagnetic Compatibility*, 48 (1): pages 187–194, 2006.
- [34] P. S. Kildal and C. Carlsson. Detection of a Polarization Imbalance including Reverberation Chambers and how to Remove it by Polarization Stirring when Measuring Antenna Efficiencies. *Microwave and Optical Technology Letters*, 34(2): pages 145–149, 2002.
- [35] Craig F. Bohren, and Donald R. Huffman. *Absorption and Scattering of Light by Small Particles*. John Wiley & Sons, Inc., 1998.
- [36] E. H. Livingston and S. Lee. Body surface area prediction in normal-weight and obese patients. *American Journal of Physiology - Endocrinology and Metabolism*, 281: pages E586–E591, 2001.
- [37] J. B. Andersen, K. L. Chee, M. Jacob, G. F. Pedersen, T. Kürner. "Reverberation and Absorption in an Aircraft Cabin with the Impact of Passengers". *IEEE Trans. on Antennas and Propag.*, 60 (5): pages 2472–2480, 2012.
- [38] P. J. Dimbylow. Fine resolution calculations of SAR in the human body for frequencies up to 3 GHz. *Physics In Medicine And Biology*, 47: pages 2835–2846, 2002.
- [39] E. Conil, A. Hadjem, F. Lacroux, M. F. Wong and J. Wiart. Variability analysis of SAR from 20 MHz to 2.4 GHz for different adult and child models using finite-difference time-domain. *Physics In Medicine And Biology*, 53: pages 1511–1525, 2008.
- [40] Akimasa Hirata, Naoki Ito and Osamu Fujiwara. Influence of electromagnetic polarization on the whole-body averaged SAR in children for plane-wave exposures. *Physics In Medicine And Biology*, 54 (2009):N59–N65, 2009.
- [41] T. Uusitupa, I. Laakso, S. Ilvonen and K. Nikoskinen. SAR variation study from 300 to 5000 MHz for 15 voxels models including different postures. *Physics in Medicine and Biology*, 55: pages 1157–1176, 2010.